



Enhancing the resolution of airborne gamma-ray data using horizontal gradients



David Beamish

British Geological Survey, Keyworth, Nottingham NG12 5GG, UK

ARTICLE INFO

Article history:

Received 30 November 2015
 Received in revised form 6 July 2016
 Accepted 6 July 2016
 Available online 7 July 2016

Keywords:

Airborne gamma-ray data
 Data processing
 Horizontal gradient
 Soil
 Geology

ABSTRACT

The spatial resolution characteristics of airborne gamma-ray data are largely controlled by survey elevation and line separation. In the UK, although low nominal survey altitudes may be permitted, regulatory zones with elevations in excess of 180 m are required above conurbations. Since the data, typically in the form of grids, are evaluated alongside many other detailed geoscientific spatial datasets their absolute resolution limits, together with their spatial characteristics, become relevant. Here, using published software, we study the theoretical resolution characteristics of this form of survey data obtained with a line separation of 200 m. Of particular interest is the airborne response behaviour when non-uniform distributions of radioactivity are encountered. Although ultimately a function of the radioelement-concentration contrast encountered, the calculations reveal that such zones are most difficult to identify when their scale length decreases below the scale of the line separation. This limited resolution then further decreases with elevation. In order to increase our ability to resolve the edges of non-uniform source regions we calculate the horizontal gradient magnitude (HGM) of the observed data. While the data used can be the estimated radioelement concentrations (potassium, thorium and uranium) or their ratios, we demonstrate that the total count is particularly suited to this type of analysis. The theoretical calculations are supported by an examination of survey data across a series of isolated bodies (offshore islands). This empirical study indicates the practical limits to resolution when using the horizontal gradient and these are governed by the survey line separation. The HGM response provides an enhanced mapping of the edges of zones associated with a contrast in flux behaviour. The edges are detected using the maxima in the response and these can be additionally examined using grid curvature analysis. The technique is assessed using recent survey data containing geological, soil and environmental influences. The results demonstrate the spatially pervasive nature of flux contrasts associated with soil and environmental contributions which potentially mask, or perturb, the underlying bedrock geological response.

© 2016 Published by Elsevier B.V.

1. Introduction

Radiometric, or gamma-ray spectrometric surveys are used to calculate concentrations of the radioelements potassium, thorium and uranium by measuring the gamma-rays which the radioactive isotopes of these elements emit during radioactive decay. The fundamentals of airborne radiometric surveys are described by Minty (1967). The geochemical interpretation of such data, in the regolith context of Australia, is discussed by Dickson and Scott (1997). Their application to soil/regolith mapping is described by Wilford et al. (1997). In the UK, airborne total gamma count surveys were first flown over SW England in 1957–9 as part of the UK Atomic Energy Authority uranium exploration programme (Kimbell et al., 2003). Higher resolution, regional scale, multi-parameter, airborne geophysical surveys commenced in 1998 (Peart et al., 2003). Since then a number of further surveys,

incorporating radiometric spectrometric data and using flight-lines spaced at 200 m have been conducted at relatively low nominal altitudes (56 to 90 m). A feature of these surveys is a regulatory requirement to increase survey elevation (to >180 m) over conurbations.

The modern surveys have been conducted for resource, soil and environmental assessments. Soils in the UK generally formed after the last ice age (<12,000 years ago) and are therefore distinct from the ancient soils of Pangea (e.g. those of Africa and Australia). Two particular aspects of gamma-ray flux behaviour arise in the case of the UK (i.e. a temperate, mid-latitude zone) and these are (a) the prevalence of a 'lower-bound' on soil moisture and (b) the occurrence of low density, organo-mineral and organic soils (Beamish, 2015). The soil, when sufficiently thick, attenuates the flux. The degree of attenuation with depth is governed by the density and wetness of the soil profile as described by Beamish (2013, 2015). The conceptual model of soil-superficial-bedrock behaviour is that the bedrock acts as a parent material to the soil so that the particle size, mineralogy and radioelement concentrations of the soil derive from the bedrock material. Significant exceptions

E-mail address: dbe@bgs.ac.uk.

may occur in the case of material transport (e.g. weathering, erosion, groundwater flow and leaching).

Since the radiometric data are evaluated alongside many other detailed geoscientific datasets the absolute resolution limits of the airborne data, together with their spatial characteristics, become relevant. In order to assess the volume of material contributing to the gamma-ray flux measured by an airborne detector, the concept of a circle of investigation was presented by Duval et al. (1971). It was found that altitude is the most important parameter in determining the volume of material that produces a given percentage of the total observed flux and the results discussed by Duval et al., (1971) are often quoted. The calculations however only relate to an infinitely large, homogenous material.

Further calculations relating to the design parameters for airborne surveys were presented by Pitkin and Duval (1980) building on the earlier work. The study included the effects of finite 'anomalous' source regions (e.g. regions of enhanced radioactivity) and therefore the calculations can be used to assess the spatial mapping capabilities for any specified airborne survey. Here we revisit the calculations of Pitkin and Duval (1980) using software made available by the U.S. Geological Survey: USGS (Duval, 1997). The calculations performed here provide detector flux responses due to finite source concentrations at survey elevations of 60 and 120 m. Here we primarily consider circular source regions (e.g. a localised soil or environmental response) and an infinite linear strip (e.g. a geological response). Linear dimensions of the source region range from 50 to 400 m and are considered in relation to a flight line spacing of 200 m. For more extensive sources, the detector response becomes uniform across the source region before the source edge modifies the response.

The behaviour of the anomalous response characteristics indicate that the lateral scale of the source response is governed by the scale length of the anomalous region. The edges of the source region are identified by the response decrease to a background value. This type of behaviour is also found in potential field data. Magnetic and gravity spatial derivatives have a well-established role in the interpretation of such data. Many methods have been developed to estimate the edge-location of singular bodies (Nabighian et al., 2005). In the same context of edge detection we here consider the behaviour of the horizontal gradient magnitude (HGM) of the anomalous radiometric response. The horizontal gradients are calculated from the set of theoretical anomaly response profiles and it is demonstrated that maxima are associated with the source edge locations except for the smallest bodies. A uniform HGM response (no horizontal gradient) is necessarily associated with extended uniform source regions. Based on these results, it is suggested that a horizontal gradient analysis of airborne radiometric data offers enhanced resolution of regions characterised by changes in concentration and hence flux behaviour.

The majority of airborne radiometric data are assessed using gridded data sets that comprise the three main radioelements (and their summary ternary image) together with their associated ratios. Additionally total count (TC) data are used to summarise the total flux observed across a broader energy range. In theory horizontal gradient analysis can be applied to any of the three individual radioelement distributions, their ratios and the total count. The radioelement concentration data and total count are one-sided, positive response measurements with a noise floor that permeates the low count behaviour. The ratio information is subject to error propagation from the constituent data and is correspondingly noisier. The horizontal gradient calculation may amplify the noise content of a particular data set and it is relevant to consider the signal to noise characteristics of the data used. In previous UK studies of the attenuation characteristics of radiometric data (e.g. Beamish, 2013) the total count, being a spectral summation, has been used to provide a high signal-to-noise ratio and is also used here in assessing the HGM response.

Since the theoretical calculations are idealised (no noise), we consider the HGM response obtained from survey data across a control

study area. The data used are total count obtained across a series of small islands in which the background material (the sea) provides a null response. The degree to which the outline of each island may be detected in the HGM edge response is demonstrated. We also assess the application of curvature analysis (Blakely and Simpson, 1986; Phillips et al., 2007) to map peak (ridge) locations determined by the HGM analysis. The control study uses high-contrast materials so that it also necessary to consider the general case of survey data which encounter more spatially-complex soil, environmental and bedrock variations. Recent UK survey data are used to study the behaviour of the HGM response. A 22 × 20 km study area from SW England provides examples of geological, soil and environmental responses and their characterisation using the HGM total count response. The study is then extended to the local scale to examine the detailed characteristics of some of the soil and environmental responses detected. Finally the HGM response obtained using total count is compared with the ternary response obtained using the HGM of the three individual radioelements.

2. Theory

2.1. Field of view

In order to assess the volume of material contributing to the gamma-ray flux measured by an airborne detector, Duval et al. (1971) introduced the concept of a circle of investigation. The authors performed theoretical calculations based on a flat homogenous material that is infinitely large and infinitely thick (the so-called infinite source). The calculations are valid for gamma-ray energies from 1.5 to 3.0 MeV and therefore for energies associated with the 3 main naturally-occurring radioelements. The effects of altitude, air and source material density together with their attenuation coefficients were investigated. It was found that altitude is the most important parameter in determining the volume of material that produces a given percentage of the total observed flux. In a more wide-ranging set of theoretical calculations, Pitkin and Duval (1980) considered the broader design requirements of airborne surveys in terms of their resolution capabilities. The parameters considered included aircraft speed, flight line spacing and detector volume. The calculations were based on the same conceptual model of the infinite source yield and circle of investigation and relate the airborne detector response to the ground area viewed by the detector. Importantly, the study included the effects of finite 'anomalous' source regions (e.g. a region of enhanced radioactivity) and therefore the calculations can be used to assess the spatial mapping characteristics for any specified airborne survey.

Duval (1997) produced a U.S. Geological Survey (USGS) report, providing and describing, a set of gamma-ray modelling programmes that are based on the previous publications and allow the user to perform their own evaluations. This software is used here to provide an understanding of UK airborne data with an elevation range from 60 to 120 m and a flight line spacing that is typically 200 m. Initially we consider a so-called strip model which extends the circle of investigation analysis to a moving detector (here we use a velocity of $64 \text{ m} \cdot \text{s}^{-1}$). Flux contributions from strips parallel to the flight path are summed in order to provide a spatial description of the areal contribution from an infinitely thick source. Secondly we consider the effects of anomalous finite gamma-ray sources. These are finite areas defined by a relative increase in their source concentration. The areas considered can be circular, rectangular or an infinite linear feature of constant width (any orientation to the flight line). The latter is probably more relevant to a geological context, although all three display similar edge behaviour in relation to the intrinsic scale of the anomalous feature. Here, for brevity, we consider circular features. The calculations use a set of defined parameters. The parameters used here are (i) a material attenuation coefficient of $0.0444 \text{ cm}^2 \cdot \text{g}^{-1}$ (e.g. at energies associated with potassium), (ii) a detector area of 0.02 m^2 , (iii) a detector photo-peak efficiency of

0.15, (iv) an air density of $0.0012 \text{ g} \cdot \text{cm}^{-3}$ and (v) a material density of $1.1 \text{ g} \cdot \text{cm}^{-3}$ (i.e. soil).

The strip calculations for a moving detector across an infinite and uniform source region are presented in a number of useful ways by Pitkin and Duval (1980). They are only partially repeated here for the sake of completeness. The cumulative percentage of total flux arising from strip widths ($2 \times$ the symmetrical radius perpendicular to the flight line) is shown in Fig. 1a for flying heights of 60, 120 and 180 m. The behaviour observed is a series of bell-type curves that allow the circles of investigation to be compared at different flying heights. Thus 90% of the total flux is obtained across scale lengths of 250 m (60 m elevation), 360 m (120 m elevation) and 440 m (180 m elevation). The same information can also be presented in a different way by extracting a set of values of the cumulative response and plotting the strip width associated with flying height as shown in Fig. 1b. The results demonstrate the degree to which airborne measurements, measured at intervals from 60 to 70 m (using typical aircraft speeds of 60 to 70 m/s) along flight lines, constitute a moving-average spatial measurement thus limiting precise resolution of flux behaviour.

Of more relevance to most survey data is the response behaviour when non-uniform distributions of radioactivity are encountered. The model considered is a finite area (a circle) defined by a relative increase in source concentration. The flight line bisects the anomalous region and the centre of the anomalous region is here set at 500 m. The source and background regions are assumed to be infinitely thick and a large relative concentration increase of 50 is used for the anomalous area. The source contributions for circles with radii from 25 to 200 m (lateral distances of 50 to 400 m) are shown in Fig. 2 for two survey heights of 60 and 120 m. The decrease in count rates with survey altitude is most evident together with a reduced response with decreasing source dimension. Obviously when considering real data and their associated errors the detectability of small anomalous areas with lateral dimensions of $< 100 \text{ m}$ is likely to be low. The half-widths (the distance across which the peak amplitude is reduced by 50%) for the data shown in Fig. 2 are summarised in Table 1.

The resolution of each feature decreases with the source dimension. The largest region (a lateral dimension of 400 m) is found to provide a half-width $> 350 \text{ m}$. Assuming a survey with 200 m flight lines that are symmetrical about the centre of the anomalous region, then the larger

area will produce a significant response across 3 flight lines (e.g. at lateral distances from 300, 500 and 700 m in Fig. 2). As the dimension of the circular body increases beyond a radius of 200 m, the source contribution becomes uniform at the peak response observed in Fig. 2. This uniform response then decays to zero towards the edges of the region and follows the spatial decay behaviour shown in Fig. 2.

We have also compared the behaviour of the infinite linear source (perpendicular to flight line) with that of the circular response discussed above. In order to compare like-with-like, we consider that a linear dimension (a width) of a linear source should be equated to the diameter of the circular source. When this comparison is undertaken it is found that the behaviour of the infinite source follows the general behaviour of the circular source (i.e. the behaviour shown in Fig. 2 and summarised in Table 1). One distinct difference is that the infinite linear source produces a larger amplitude response for the same source concentration contrast (when the survey line is perpendicular to the source strike). This implies that, for the same source concentration contrast, an extensive linear anomaly (i.e. a geological anomaly) is more detectable than an equivalent circular feature (i.e. a localised environmental anomaly).

2.2. Horizontal derivatives

The behaviour of the anomalous response characteristics shown in Fig. 2 indicates that the lateral scale of the source response is governed by the scale length of the anomalous region. The edges of the source region are then identified by the response decay to a background value (a value of zero in this theoretical case study). This type of behaviour is also found in potential field data. Magnetic and gravity spatial derivatives have a well-established role in the interpretation of such data (Grauch et al., 2001) but can also be usefully applied to non-potential field data (Beamish, 2012). The source parameters that are typically estimated are the boundaries or edges of singular source bodies (Blakely, 1995; Blakely and Simpson, 1986). In the same context of edge detection we here consider the behaviour of the horizontal gradient magnitude of the anomalous response.

The horizontal gradients calculated from the set of anomaly response profiles of Fig. 2 are shown in Fig. 3. The symmetrical behaviour displays a minimum at the origin of the anomalous region (located at

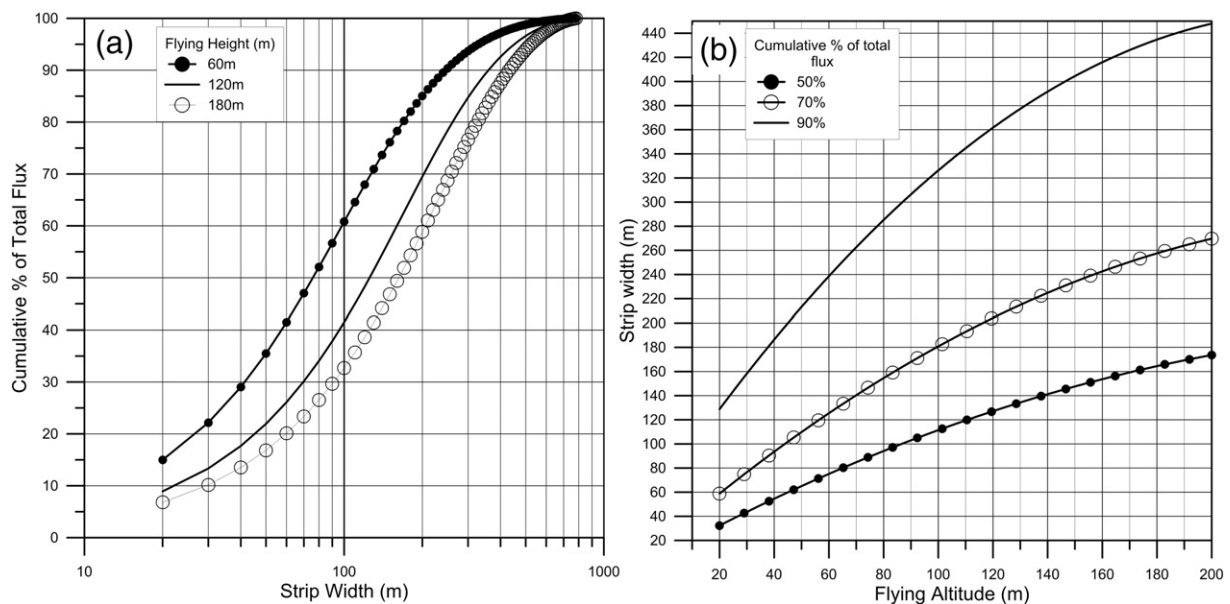


Fig. 1. Results of the strip calculation for a moving detector across a uniform half-space. (a) Cumulative % of total flux as a function of strip width for 3 survey heights. (b) Variation of fixed cumulative % of total flux as a function of strip width and survey height.

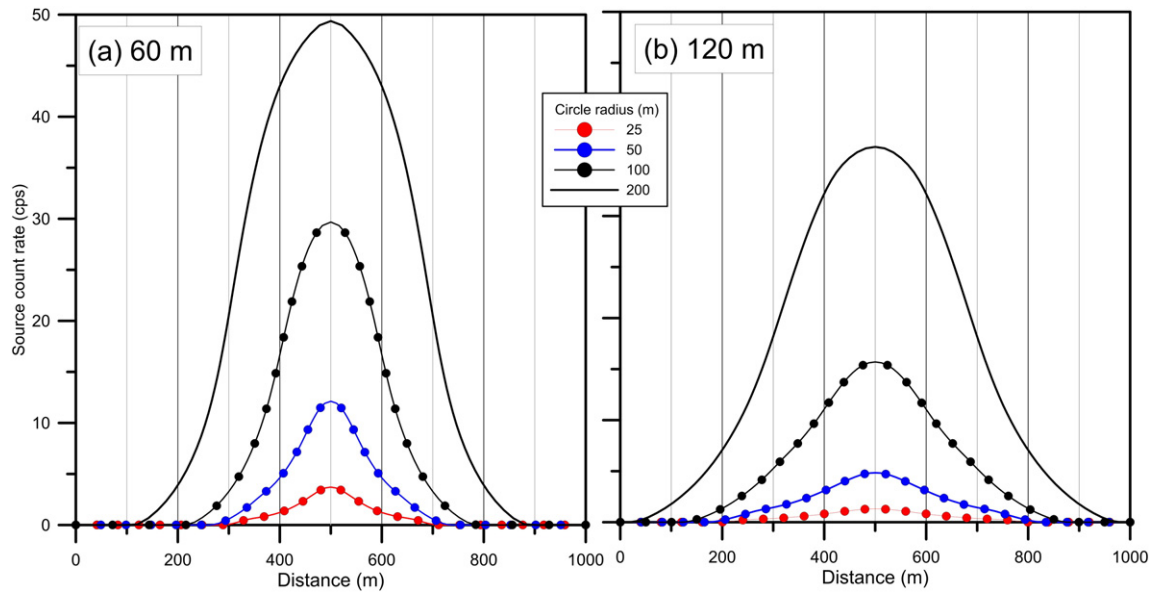


Fig. 2. Variation of detector count rate for circular source regions with radii from 25 to 200 m and centred at 500 m. (a) 60 m survey height. (b) 120 m survey height.

500 m). Maxima are then observed towards the edges of the anomalous region. At a survey elevation of 60 m (Fig. 3a), the maxima are observed at the edge locations of each circular region for radii of 200 m, 100 m and 50 m. The maxima for the 25 m circle are close to those of the 50 m model and probably indicate a resolution limit has been reached in the calculations employed. The behaviour is repeated at a survey elevation of 120 m for radii of 200 m and 100 m, but the spatial gradients are less distinct for radii of 50 and 25 m due to the low amplitudes of the response used in the calculation. Shoulders appear in the gradient response beyond the position of maximum amplitude. The shoulders become increasingly significant both with decreasing body size and increasing elevation. The results indicate the likely practical limits of small body detection when using 200 m flight lines obtained with an envelope of survey elevations (rural and conurbation).

For larger bodies the horizontal gradient response is a minimum over the source region (the response is uniform over the source region and produces no horizontal gradient). Horizontal gradients are then produced across the edges in accord with those observed in Fig. 3. It is suggested that a horizontal gradient analysis of airborne radiometric data offers enhanced resolution of regions characterised by a change in concentration and hence flux behaviour. The analysis is summarised in Fig. 4 which considers a circular anomaly with a radius of 100 m and plots the response behaviour, observed at 60 m, as a 3D perspective view. The source detector response (Fig. 2a) is shown as a wireframe and the high values of the horizontal gradient response (Fig. 3a) are shown as a colour contour plot. The peak in the horizontal gradient is a circle which is associated with the body edges.

Thus far we have considered only idealised (no noise) data. In contrast to potential field data, the gamma-ray data are positive response measurements with a noise floor that permeates the low count

behaviour and limits the idealised resolution characteristics. In theory horizontal gradient analysis can be applied to any of the three individual radioelement distributions, or their ratios. The horizontal gradient calculation may amplify the noise content of a particular data set and it is relevant to consider the signal to noise characteristics of the data used. A horizontal gradient analysis may be applied to line-based (profile) data or to gridded data sets. When a grid analysis is undertaken, the total horizontal gradient magnitude (HGM) is based on the x-derivative (dx) and y-derivative (dy) responses and is defined as the positive-only response:

$$\text{HGM} = \sqrt{(\text{dx})^2 + (\text{dy})^2} \quad (1)$$

The HGM is commonly referred to as an edge-detection filter and is widely used in geophysical interpretation (e.g. Grauch et al., 2001).

3. Materials and methods

3.1. The airborne radiometric data

Here we use UK airborne radiometric data sets obtained with a line-separation of 200 m which were obtained at low elevation, subject to regulatory increases in elevation above conurbations. A small (3×3 km) control data set is taken from the Tellus survey of Northern Ireland (2005–2006) described by Beamish and Young (2009). A larger study area is extracted from the TellusSW survey flown in the latter half of 2013 and described by Beamish and White (2014). In both surveys, a radiometric data sampling of 1 Hz provides an along-line sampling largely in the range from 60 to 70 m.

The radiometric data were acquired with a 256 channel gamma spectrometer system (GeoExploranium GR-820/3) comprising 32 l of downward-looking NaI(Tl) detectors and 8 l of upward-looking detectors. Uranium (^{238}U) is estimated through the radon daughter ^{214}Bi in its decay chain, while thorium (^{232}Th) is estimated through ^{208}Tl in its decay chain. Potassium (^{40}K) is measured directly at 1.461 MeV. Conventionally secular equilibrium in the decay chains of uranium and thorium is assumed (Minty, 1967) and the ground concentration results are reported as equivalent uranium (eU, ppm) and equivalent thorium (eTh, ppm). Potassium is reported as %K. Total count (TC) data (energy

Table 1

The half-widths (the distance across which the peak amplitude is reduced by 50%) for the data shown in Fig. 2 for elevations of 60 and 120 m.

Body radius (m)	60 m half-width (m)	120 m half-width (m)
25	140	250
50	160	260
100	216	300
200	370	392

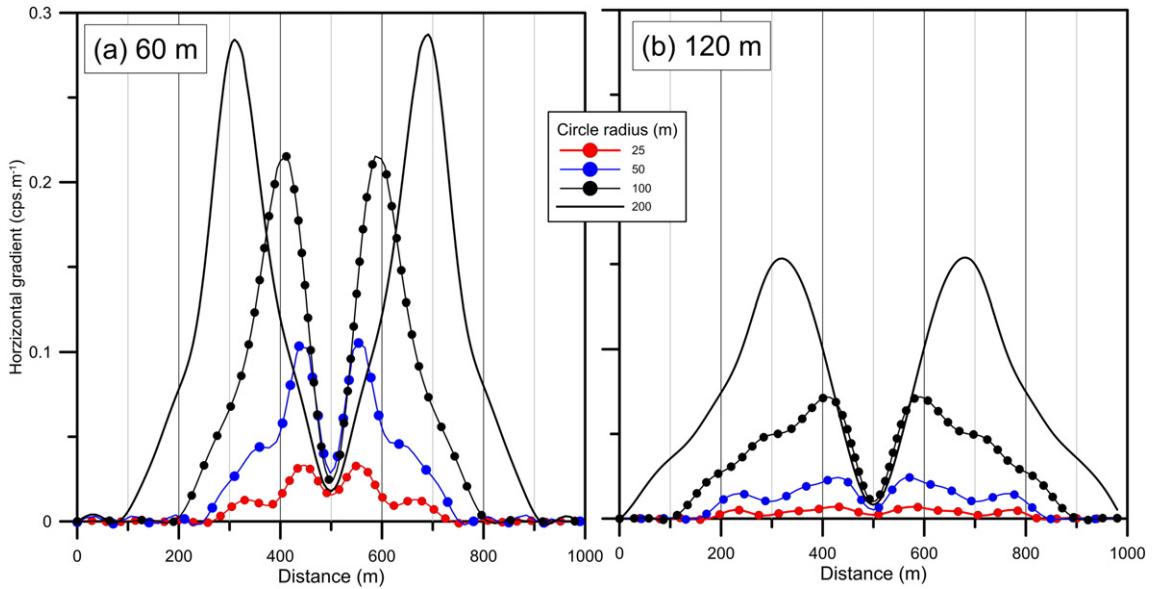


Fig. 3. Horizontal gradients calculated from the detector response functions of Fig. 2. Circular source radii range from 25 to 200 m and are centred at 500 m.

range from 0.41 to 2.81 MeV) is reported in cps. A vertically uniform activity concentration is assumed.

The gamma radiation registered by the detector is composed of contributions from soil/rock, the atmosphere, the aircraft and cosmic radiation. In order to calibrate airborne radiometric data, the commonly adopted standard is to follow the recommendations made in a series of technical documents and publications from the International Atomic Energy Agency (IAEA). The set of procedures applied here are based on protocols described in IAEA (1991, 2003, 2010) and by Grasty and Minty (1995).

The zero-level characteristics of the processed radiometric data were obtained from survey data over deep water. In the case of

Northern Ireland data, the standard deviation of the total count null data was reported to be 40 cps. In the case of the TellusSW data, the figure increases to 76 cps.

3.2. Data processing

Guidelines for the mapping of radiometric data have been published (IAEA, 2003) and these indicate the most frequently used algorithms are the bi-directional gridding and minimum curvature techniques. Kriging has not been widely used as it is difficult to account for the anisotropy in the sample density when modelling the semivariogram. Here the grids are obtained using a minimum curvature algorithm which produces a

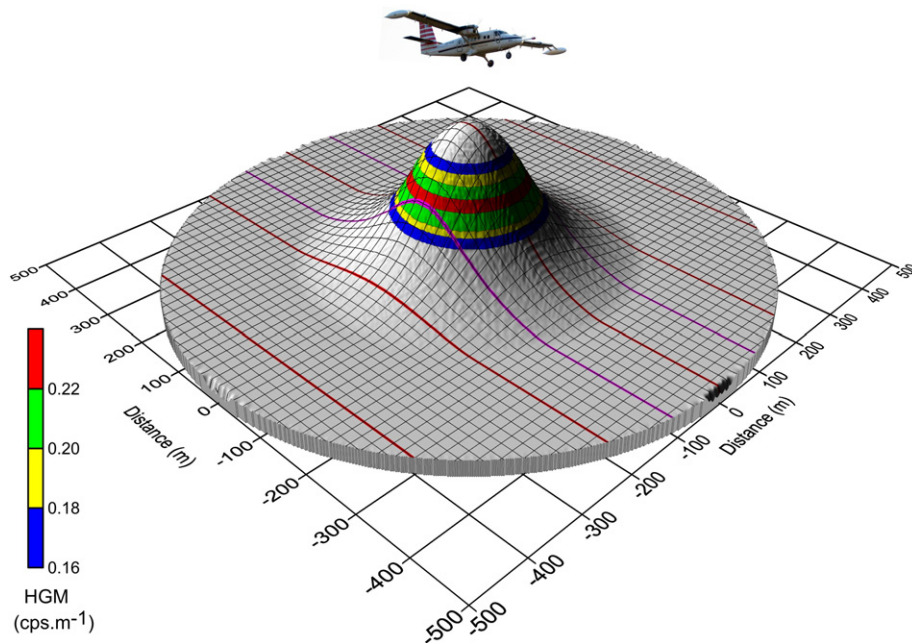


Fig. 4. 3D perspective view of the detector count rate response (greyscale and wireframe) and high values of the horizontal gradient magnitude (HGM), values $>0.16 \text{ cps}\cdot\text{m}^{-1}$. Survey elevation is 60 m. The source circle has a diameter of 200 m and is centred at the origin. The aircraft and altitude, representing the detector, are not to scale.

smooth grid by iteratively solving a set of difference equations minimising the total second horizontal derivative while attempting to honour the input data.

For the analysis conducted here we use minimum-curvature grids with a cell-resolution of 40 m. Having obtained a gridded data set of the HGM response, a common processing procedure is to extract the maxima of the HGM response as described by Blakely and Simpson (1986). The methodology was further considered by Phillips et al. (2007). These authors employed a 3×3 (grid cell) moving-window to assess the local curvature and define turning points. Here we use a ridge analysis to isolate maxima. The application of these procedures to the HGM estimates from TC data, and the individual radioelements, to improve edge detection of anomalous source regions, is also considered.

4. Results

4.1. A control example

Ideally the detection and resolution limits of TC data and their associated horizontal gradients could be demonstrated using data obtained across isolated zones of varying sizes. In the UK, many airborne surveys

contain an offshore extension to accommodate the acquisition of magnetic data. Offshore islands then offer isolated zones with a given TC (soil-geological) response with a surrounding sea providing a null (theoretically zero) response. Survey data across a 3×3 km area in Northern Ireland, comprising a number of islands, typical of drowned drumlin topography, were used by Beamish (2012) to study the resolution characteristics of airborne electromagnetic data. Here the same area is studied in relation to the radiometric TC response. The islands lie within the tidal Strangford Lough on the eastern seaboard. The area is shown on a base topographic map in Fig. 5a with the onshore area appearing in the west. Fig. 5 also shows the sampling locations of the airborne survey which used 200 m flight line separations at an azimuth of 345° . One advantage of this type of area is that there are only small survey elevation adjustments rather than the sometimes large adjustments that may occur across coastal cliffs. The mean survey elevation across the area was 56 m with a standard deviation of 10 m. The average distance between survey points is 52 m. The noise level of the TC data was estimated using a portion of the data entirely confined to a larger area of the sea. These data provided a typical close-to-normal distribution with a mean value of 169 cps. The full range of the null data was from 34 to 229 cps. The along-line TC data are shown as four range colour values in Fig. 5b. The 2 lowest count ranges define a potentially noise

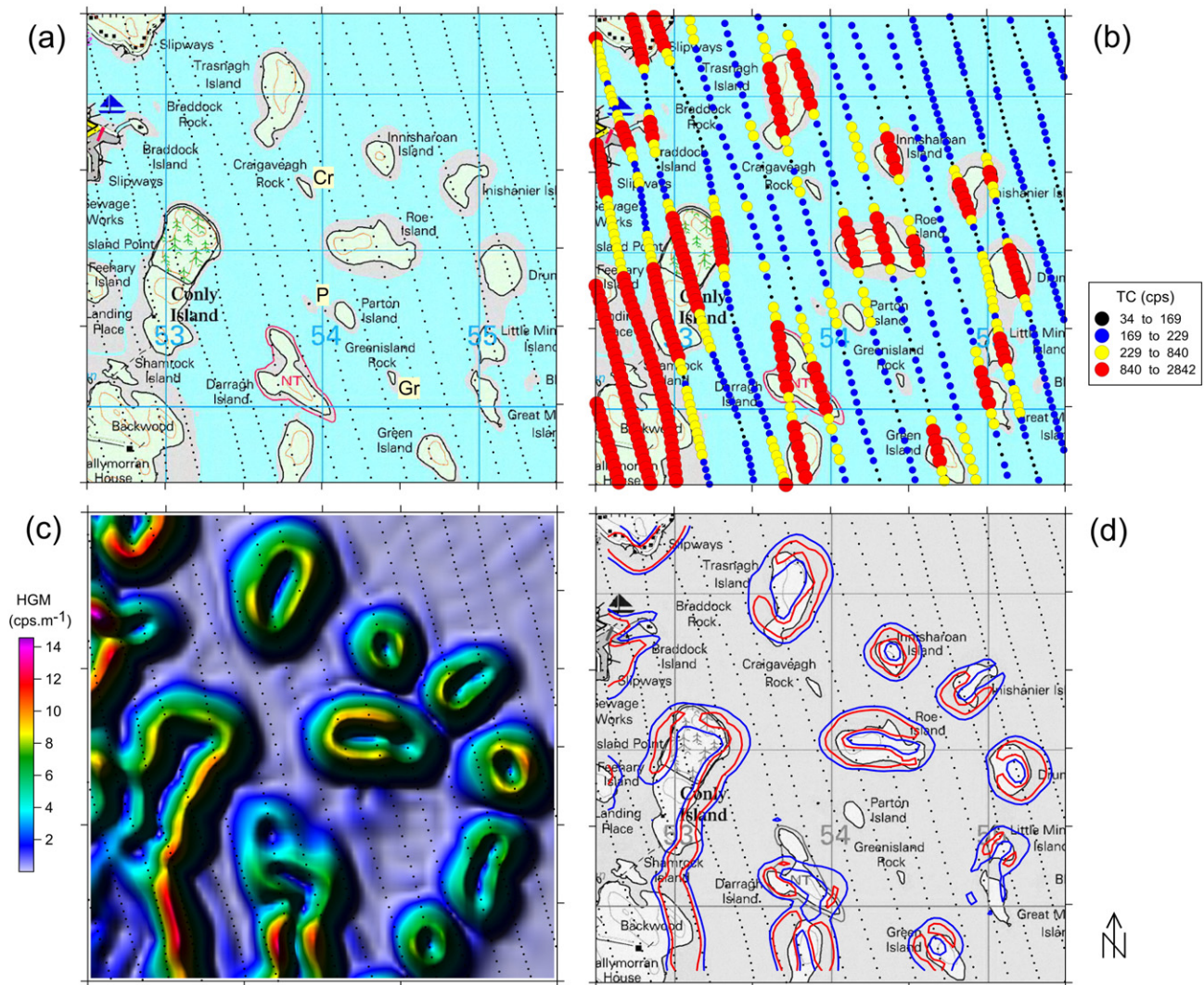


Fig. 5. The 3×3 km control study area in which the survey sample points (200 m line spacing) are shown as dots. (a) Topographic base map with the 3 smallest islands/rocks identified as Cr (Craigeaveagh rock) Gr (Greenland rock) and P (Parton Island). (b) Total count data shown as 4 colour-range posted values. (c) Continuous colour image, with shade, of the horizontal gradient magnitude (TC data). (d) Background grey-scale topographic map and two contours of the horizontal gradient magnitude, $6 \text{ cps} \cdot \text{m}^{-1}$ in blue and $8 \text{ cps} \cdot \text{m}^{-1}$ in red.

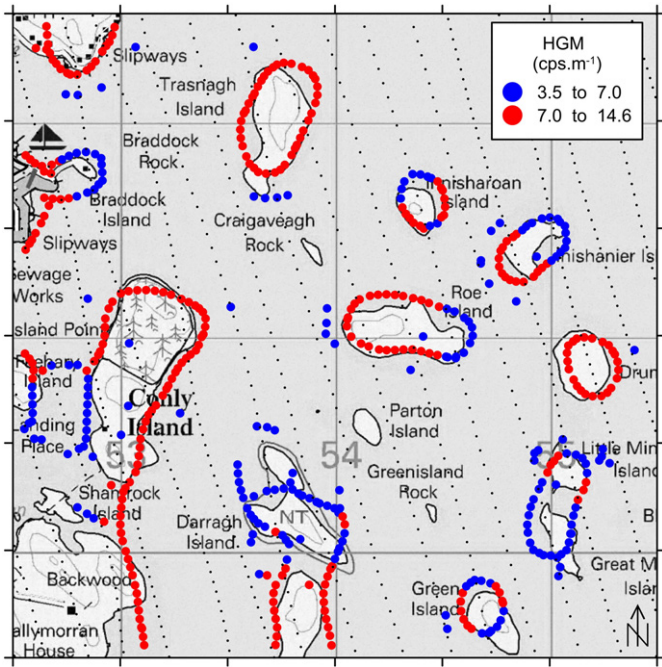


Fig. 6. The 3 × 3 km control study area in which the survey sample points (200 m line spacing) are shown as dots. Posted values of the largest amplitudes (>3.5 cps · m⁻¹) of the curvature-ridge-analysis of the horizontal gradient magnitude (TC data).

(or null) level below and above the mean value of 169 cps. The two higher ranges should then represent increasing (above noise) response behaviour.

The mainland and larger islands are all associated with high TC responses. We are not particularly interested in the precise amplitude levels but rather their decay to a zero response as indicated by the third class interval (yellow). These decays can be observed both

along-line and on adjacent over-sea lines reflecting the spatial sensitivity of the response behaviour. The smallest island is a rock (Gr, Fig. 5a) and is located midway between flight lines and no response is observed. The larger Parton Island (P) is also situated midway between flight lines and this produces a small muted response as does Craigaiveagh rock (Cr) to the north. The response behaviour across the set of islands can be further studied manually to arrive at an empirical estimate of a circle of investigation in relation to the edge of these isolated bodies. In detail the edge of each body is not precisely defined due to the occurrence of sand beaches. Despite this the analysis suggests that, for these TC data, the lateral distance across which the response is reduced by 90% ranges from 42 to 182 m with a mean of 101 m.

The HGM response of these data is shown as a continuous colour (linear) image in Fig. 5c. The high amplitudes clearly outline the flux contrasts provided by the land-sea edges. The 3 smaller rock-island features, previously noted, do not provide a significant HGM response. In order to clarify the behaviour of the HGM, Fig. 5d shows two high contour levels (6 and 8 cps · m⁻¹) of the HGM response and shows more clearly the extent to which the edges of individual islands are resolved. The application of the curvature-ridge analysis of Phillips et al. (2007) applied to the HGM response is summarised in Fig. 6. This form of moving-window analysis is known to produce a level of spurious behaviour in the ridge solutions obtained. Here we retain only the highest amplitudes (HGM > 3.5 cps · m⁻¹) for evaluation. For these data we note that the ridge solutions (and indeed the HGM) can only partially replicate the complex spatial form of the islands and the associated changes in radiometric contributions. Comparing Fig. 5c, d and Fig. 6 we note that the continuous image of the HGM is potentially the most useful in providing the largest dynamic range of the behaviour generated by the lateral contrasts.

The coastal example obviously provides high levels of flux contrast which are unlikely to be representative of the behaviour of the majority of survey data. We now consider further soil, geological and environmental examples taken from a recent airborne geophysical survey of SW England. We note that when examined at the detailed scale (as

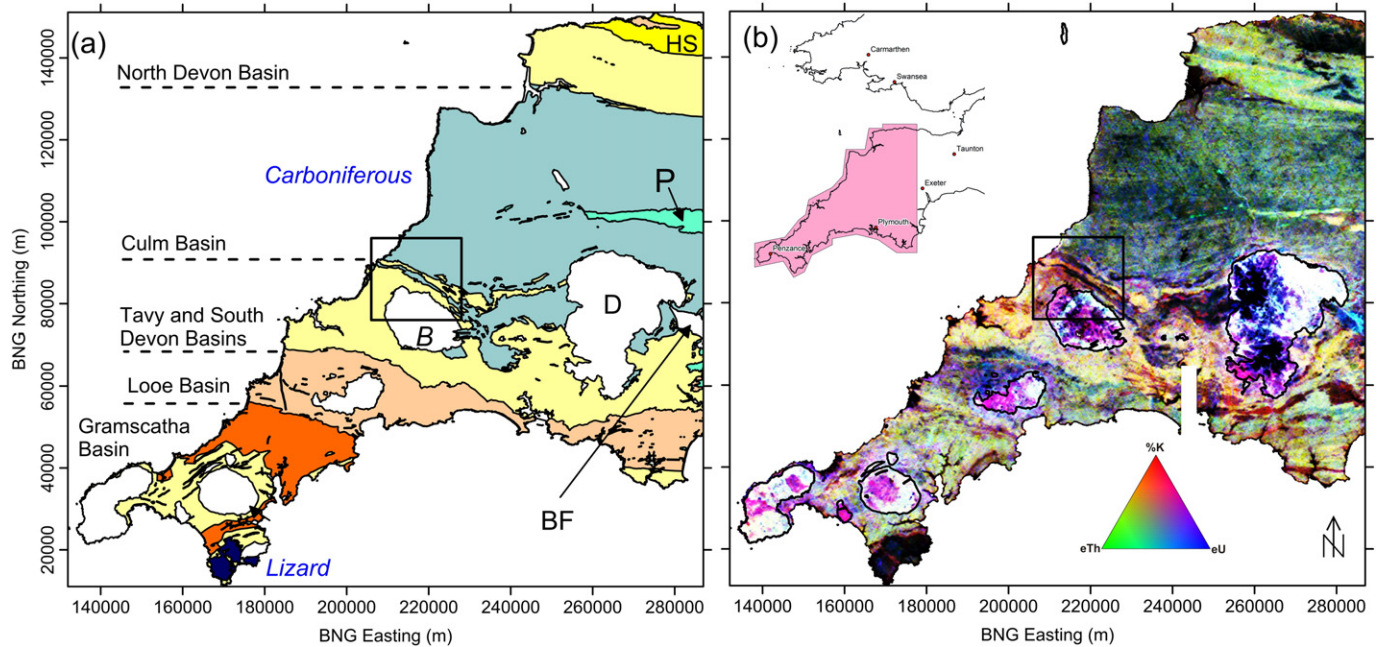


Fig. 7. TellusSW survey area and location map (inset). Central rectangle identifies the main study area. BNG refers to British National Grid. (a) Simplified geology based on basins identified by Leveridge and Hartley (2006). HS: Hangman Sandstone formation, P: Permian formation, BF: Palaeogene Bovey Formation. Five outcropping granites are identified in white, B (Bodmin) and D (Dartmoor). (b) The radiometric ternary colour image obtained using the 3 radioelement ground concentrations.

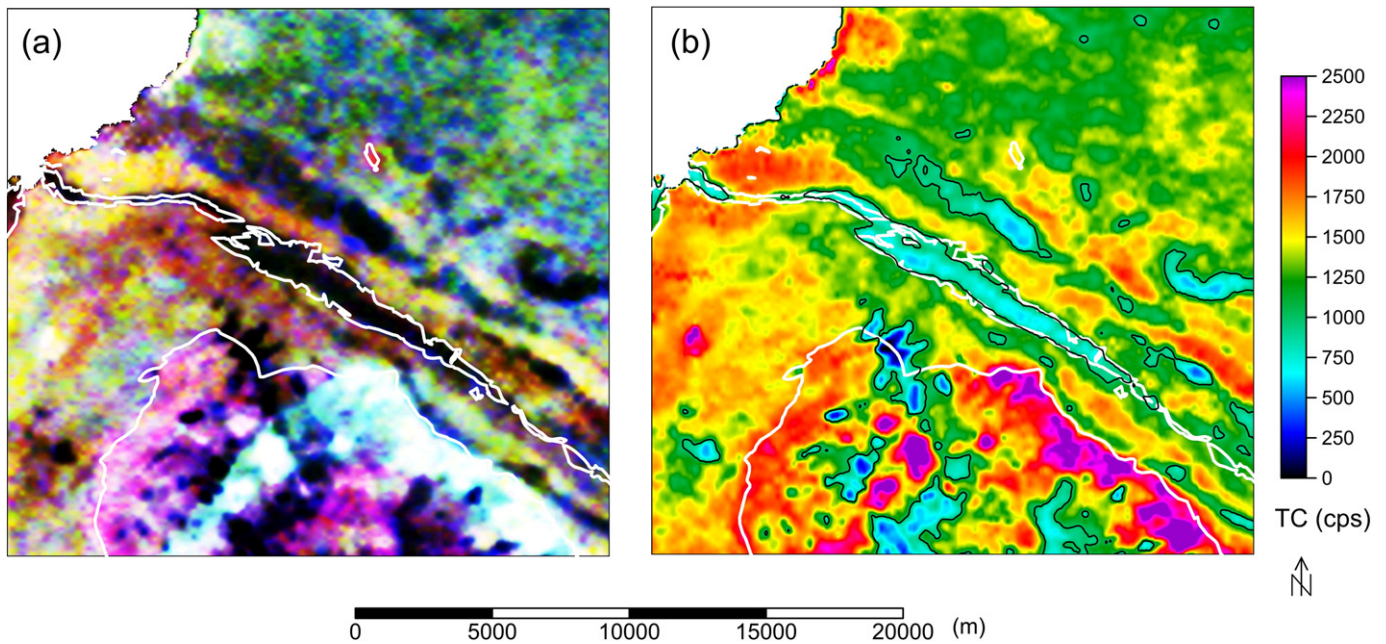


Fig. 8. The 22×20 km main study area with outlines of the Bodmin granite outcrop and the Tintagel volcanic formation in white. (a) Ternary image, legend as in Fig. 7. (b) Total count image using a linear scale. A single black contour identifies a value of 1000 cps.

above), the HGM response is unlikely to provide an exact edge, or boundary, description of the flux contrast when compact and spatially complex areas are encountered.

4.2. Whole survey

The radiometric data from the TellusSW survey is displayed as a ternary image alongside a simplified version of the bedrock geology in Fig. 7. A granite batholith intruded the existing country rock during the Variscan Orogeny producing metamorphic zones and establishing fluid circulation zones responsible for the extensive polymetallic mineralisation of the region (Edmonds et al., 1975). Fig. 7a shows the

granite outcrops in white. The majority of the metasediments are pelites or graywackes and are of Devonian age although a large extensional, structure preserved Carboniferous sediments as the Culm Basin (Fig. 7a). Following Leveridge and Hartley (2006) a sequence of basins are identified in Fig. 7a to allow comparison with the radiometric data. A 22×20 km rectangle identifies the study area considered here which covers part of a granite (Bodmin, B in Fig. 7a) and the Devonian-Carboniferous contact area.

The ternary image (Fig. 7b) is a 3-way colour stretch formed from the distributions of potassium (red), thorium (green) and uranium (blue). The image is cut-to-coast to remove the null responses over the offshore area. White responses indicate areas in which all three

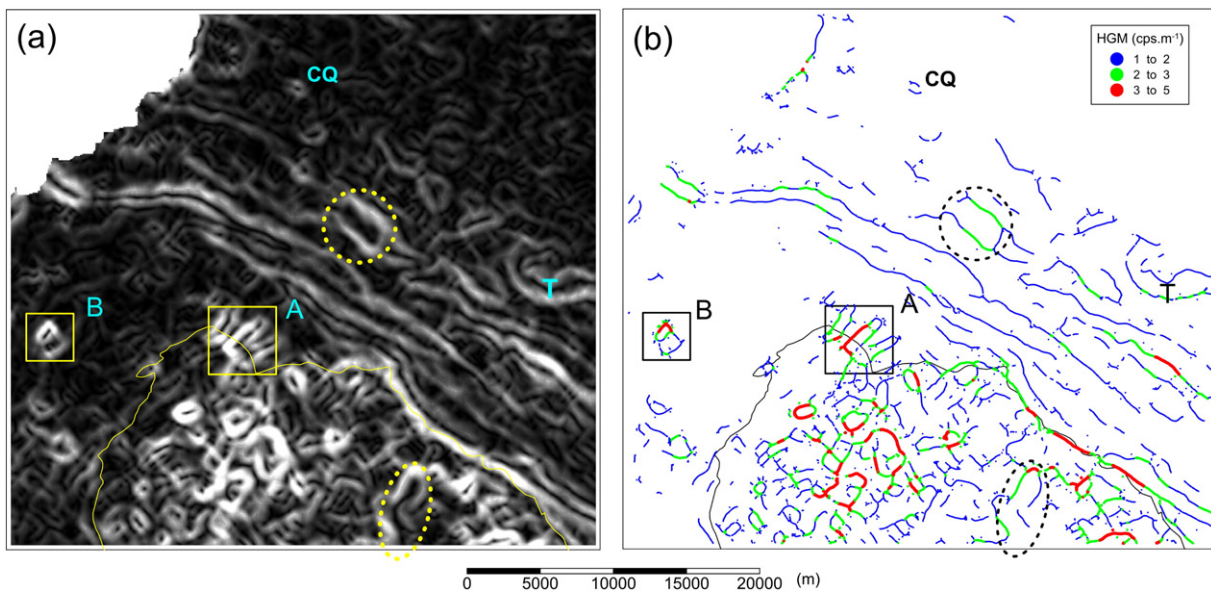


Fig. 9. The 22×20 km main study area with outline of the Bodmin granite outcrop. Two regions with dotted outlines are extensive zones of woodland. T refers to a response associated with one outcrop of the Teign chert formation. CQ refers to Cansford quarry. Two rectangles labelled A and B define 2 further study areas. (a) Continuous grey-scale image of the horizontal gradient magnitude (TC data) with black representing zero and white representing a maximum value. (b) Curvature ridge analysis of the horizontal gradient magnitude showing values above $1 \text{ cps} \cdot \text{m}^{-1}$.

radioelements have high concentrations while black responses represent lows. The zones with the highest radiometric responses are associated with, and largely confined to, the outcropping highly radiogenic granite zones. Within the granite outcrops, areas of preferential potassium enrichment (i.e. biotite granite) are observed. It is worth noting that the radiometric data across the Bodmin granite have identified a previously unknown internal edge, clearly defined by high values, within the outcrop (see also Fig. 8). Low value responses occur in association with the ultramafic Lizard ophiolite complex and, in the north, with a Devonian lithology named the Hangman Sandstone (HS) formation which has a specific deltaic origin. Other contrasting response characteristics are observed with the Permian (P) lithologies associated with the Crediton Trough and the Palaeogene Bovey Formation (BF) in the east.

Comparing Fig. 7a and b it is evident that, at the large scale shown, the bedrock formations control the spectral response (colour) of the radiometric data. Within this framework many other detailed variations are observed. Within the Bodmin (B) and Dartmoor (D) granites low responses are caused by significant areas of peat formed on the high ground (moors) above the granites. The largest area of attenuation is due to blanket bog covering the majority of the western portion of the Dartmoor granite. In order to fully understand the radiometric response observed the role of both soils and bedrock must be considered. The

selected 22×20 km sub-area contains a complex mix of geological, soil and environmental radiometric responses.

4.3. Main study area

The ternary image and total count response across the study area are shown in Fig. 8. Although the area is relatively rural, survey altitudes range from 55 to 257 m, with a median of 85 m. The higher values are associated with conurbations. Both images reference the Bodmin granite outcrop in the south (see also Fig. 7) and a detailed (1:50 k) bedrock mapping of a single extensive Carboniferous volcanic unit (the Tintagel formation) which influences the radiometric response. The 1:50 k bedrock mapping across the area is particularly complex and fragmented so a single unit is used as an example of a geological response. The Tintagel volcanic formation (identified in Fig. 8) comprising lava, tuffs and agglomerates, crosses the entire area and is identified by a low count response (<1000 cps). The ternary image of Fig. 8a clearly provides a variety of information on the radioelement concentrations of the area both at a regional and local scale. The Bodmin granite response appears spatially complex as are all the highly radiogenic granites of the survey region (Fig. 7b). A major internal edge is apparent within the outcrop but a large number of small scale features appear to perturb the

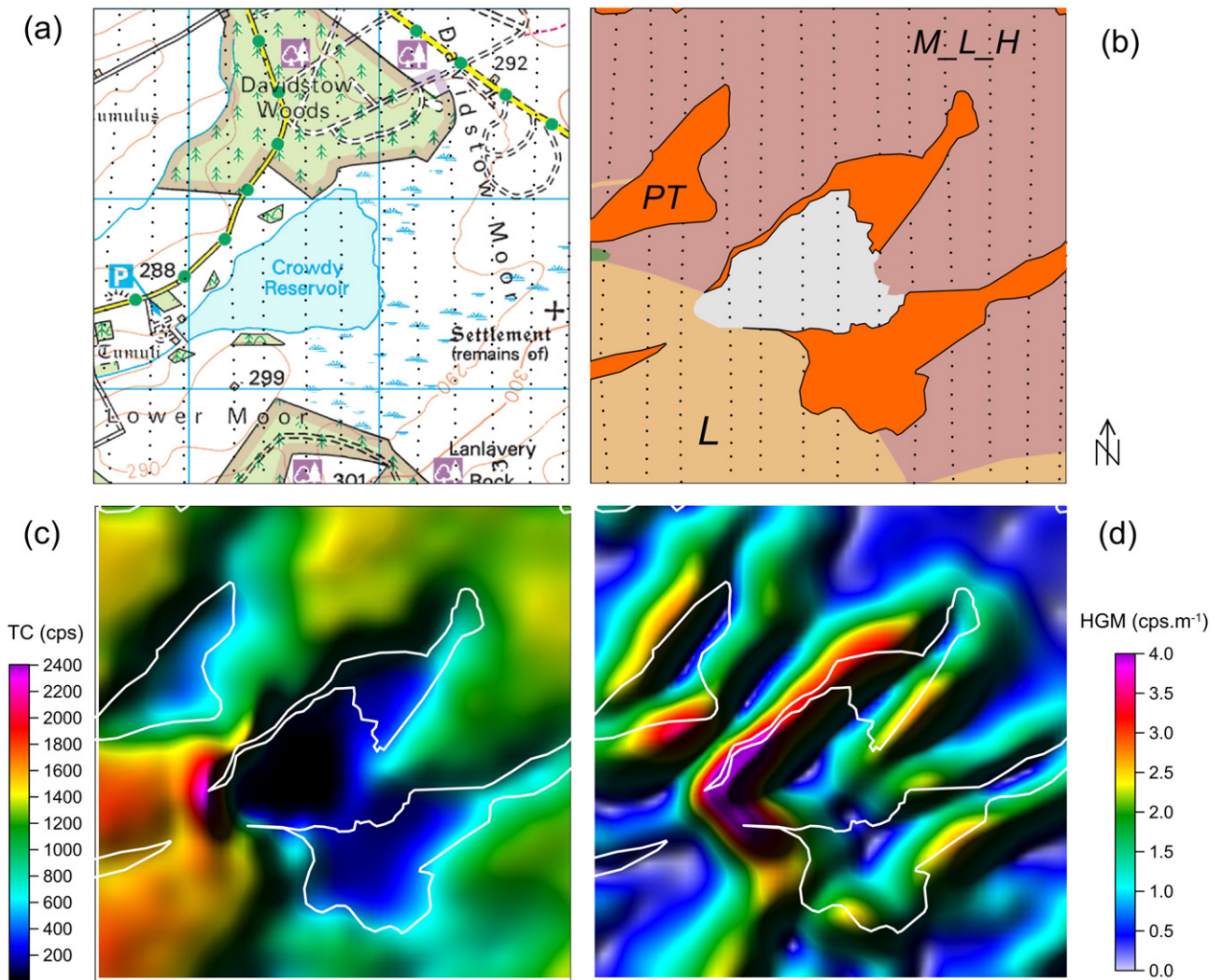


Fig. 10. The 2.5×2.5 km sub-area A. (a) Topographic base map with survey sample points as dots. (b) Soil map showing water body, zones of peat (PT), light soils (L) and medium to light (silty) to heavy soils (M_L_H). (c) Continuous colour image, with shade, of the total count (TC). (d) Continuous colour image, with shade, of the horizontal gradient magnitude (HGM) obtained from the TC data.

response. A clear and continuous granitic edge is only defined along the eastern margin of the granite.

An image of the HGM response is shown in Fig. 9a alongside a classification of the largest HGM ridge amplitudes (Fig. 9b). The grey-scale image of Fig. 9a attempts to preserve the dynamic range of the response with black representing a value of zero and pure white representing a maximum value. The colour-coded classification of the curvature-ridge analysis values associated with the data (Fig. 9b) provides a useful simplification of the information in which the lower amplitude responses are omitted. While the classified ridge amplitude data are of immediate interest (the edges that are most clearly defined) we note the lower amplitude characterisation of the HGM (Fig. 9a) also warrants assessment.

Studies of UK radiometric data (e.g. Beamish and White, 2011; Beamish, 2015) have highlighted the spatially-complex nature of their radioelement and attenuation characteristics. The HGM, as calculated here, should provide edge detection of anomalous areas defined as having higher or lower relative flux characteristics (a flux contrast). The amplitude of the TC data must therefore be used in conjunction with the HGM information. The radiometric data carry information on both bedrock geology and soils and these may also be perturbed by near-surface environmental influences (e.g. water bodies and mineral extraction sites). When providing an assessment of bedrock radioelements, all

non-bedrock responses can be considered noise. The pervasive nature of the many localised bodies identified by the HGM suggests the scale of the problem that will be encountered when radioelement information (e.g. Fig. 8a) is used in a bedrock assessment.

The HGM information, as shown in Fig. 9 may be used, alongside the conventional radiometric measurements, in conjunction with a range of additional geoscientific information (e.g. soil parent material, land-use and vegetation). Since the edge information for the area is extensive and complex only some comments and two detailed examples are provided here. Edges associated with one of the more extensive geological responses (the Tintagel volcanic zone shown in Fig. 8) are mapped across the area and some low amplitude internal boundaries within the formation are detected. A series of sub-parallel geological edges appearing to the NE of the granite are also resolved. There are other bedrock HGM responses and a closed boundary defining one area of the Teign chert formation is identified at T. Two areas, shown with broken lines in Fig. 9, show an association with 2 of the larger areas of mixed conifer and broadleaf woodland. The attenuated response across certain woodland zones remains enigmatic since not all such features give rise to the effect (Beamish, 2015).

We have chosen 2 areas, identified by rectangles in Fig. 9, to illustrate the detail contained in the HGM response. The high spatial density of small scale effects across the granite outcrop is partially related to

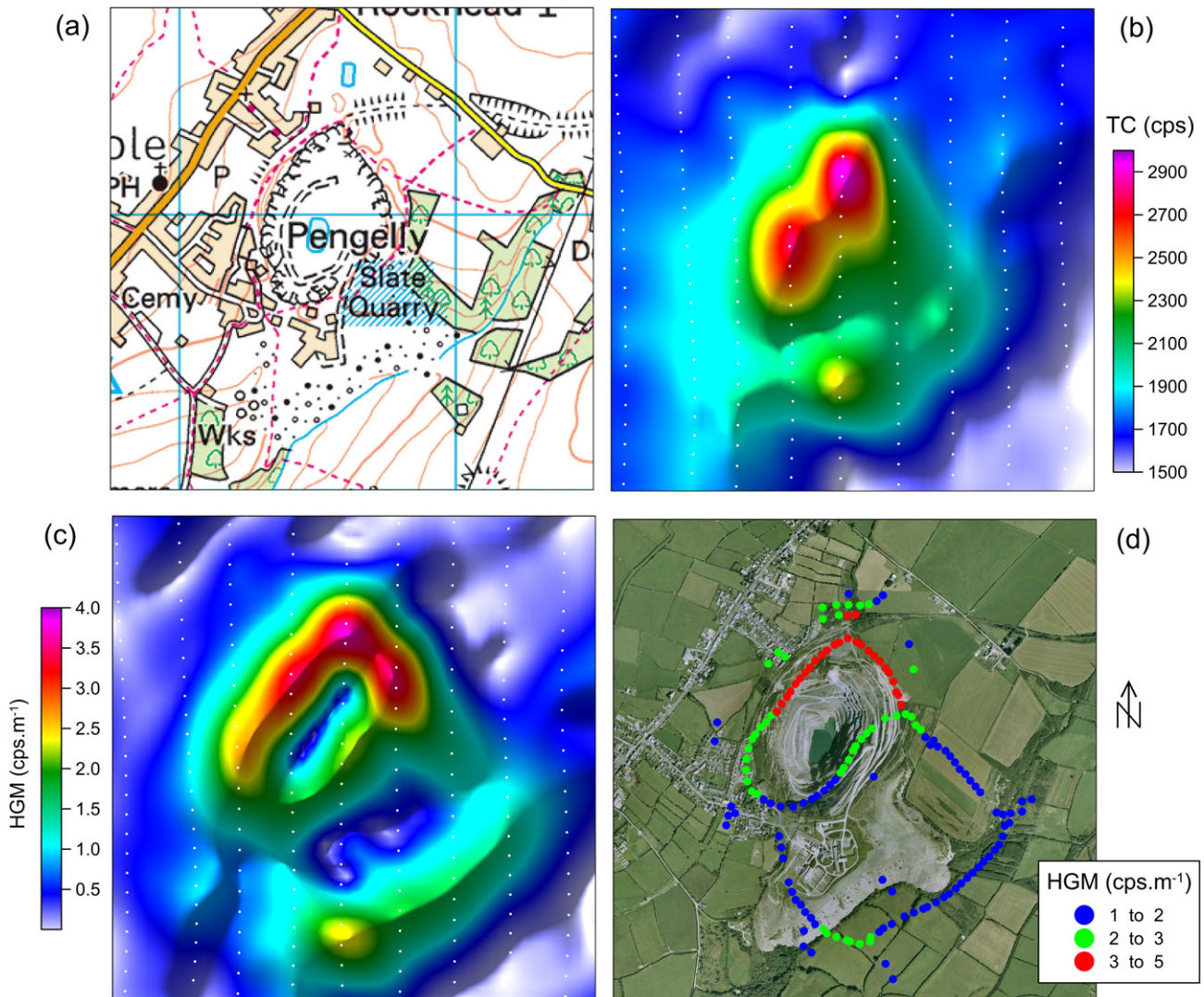


Fig. 11. The 1.75×1.75 km sub-area B. (a) Topographic base map. (b) Continuous colour image, with shade, of total count (TC), white dots denote survey sample points (c) Continuous colour image, with shade, of the horizontal gradient magnitude (HGM) obtained from the TC data, white dots denote survey sample points. (d) Curvature ridge analysis of the horizontal gradient magnitude showing values above $1 \text{ cps} \cdot \text{m}^{-1}$.

zones of wet peat. Rectangle A defines a 2.5×2.5 area across the granite margin used as an example of an attenuation effect. Zones of enhanced concentration are also observed in the HGM response. Rectangle B defines a 1.75×1.75 km area where an absence of soil cover across a quarry site generates an enhanced response. A second quarry enhancement location (Cansford quarry, CQ) is also identified in Fig. 9.

4.4. Sub-area A

A topographic base map of the 2.5×2.5 km sub-area is shown in Fig. 10a. The survey elevations range from 66 to 98 m with a median value of 81 m. Measurement locations are identified with symbols in Fig. 10a,b. The presence of the central water reservoir complicates the data assessment due to the absence of a subsurface response. Two woodland areas can also be noted and these appear not to perturb the response characteristics. The main influences on the radiometric data are compact areas of peat. The 4 peat areas, as mapped by a 1:50 k BGS (British Geological Survey) superficial cover database, are shown in Fig. 10b with a background soil texture map identifying light soils (L) associated with the granite and medium to light (silty) to heavy soils (M_L_H) elsewhere. The change in soil type also identifies the granite margin. Any potential change in bedrock response across the margin is effectively masked by the soil response. The boundaries of the peat areas are retained for reference in the following two images. Fig. 10c shows the TC data which approach, but do not reach a value of zero over the central water body. The 3 larger peat areas provide attenuation zones while the smaller peat area in the SW produces only a small reduction in amplitude. The water body edges inevitably produce the largest HGM response shown in Fig. 10d. Here the maximum HGM amplitude is seen to track the peat outlines in a reasonable manner. In detail the results suggest that the mapped peat zone in the NW extends to the NE below the conifer forest. The ability of the UK radiometric data to provide mapping of peat zones was previously described by Beamish (2014).

4.5. Sub-area B

Delabole slate quarry near Pengelly has operated continuously since the 15th century. A topographic base map of the area is shown in Fig.

11a in which a small water body can be observed at the quarry centre. Soils and bedrock across the 1.75×1.75 km area are uniform. The total count response is shown in Fig. 12b and amplitudes are enhanced across the main pit and along the spoil zone to the south (see also Fig. 12d) where soil is absent or thin. A localised larger amplitude feature is observed on the edge of the spoil zone. The HGM response shown in Fig. 12c and the HGM ridge-analysis of Fig. 12d, define a closed body around the main quarry and a subsidiary, lower amplitude feature beyond the edge of the spoil zone. It should be noted that although the depth of this quarry is exceptional (> 140 m), similar total count enhancements are routinely observed at most larger quarry sites in the UK (see also CQ in Fig. 9) and are interpreted as being due to the absence of soil cover.

5. Discussion

Although the application of HGM analysis has been demonstrated using total count data, it was previously noted that the technique can be applied to individual radioelement distributions. When undertaking such an analysis the lower signal-to-noise of these distributions, particularly that of uranium, needs to be acknowledged. Despite this, the spectral response of the HGM applied to the individual data may be considered useful. We return to the main study area for this analysis. The TC-HGM response is shown in Fig. 12a as a continuous colour image and provides a reference for Fig. 12b. The ternary image obtained from HGM-potassium, HGM-thorium and HGM-uranium for the main study area is shown in Fig. 12b. The ternary response RGB colour scale is the same as that used in Fig. 7b. In Fig. 12b there is a degree of 'colour bleeding' mainly in the blue (uranium) channel due to the higher comparative noise level in the uranium channel. Despite this, edges in the ternary-HGM response clearly track those in the TC-HGM response and display a range of spectral characteristics. In the case of the regionally-extensive geological responses, a centre-line of the zone (s) is defined in black with edges defined by a spectral response (towards yellow) that indicates the absence of a uranium (blue) component edge. The white responses in Fig. 12b result from relative highs in all 3 radioelements although subtle variations in spectral character are observed. Thus a slight thorium enhancement is seen in association

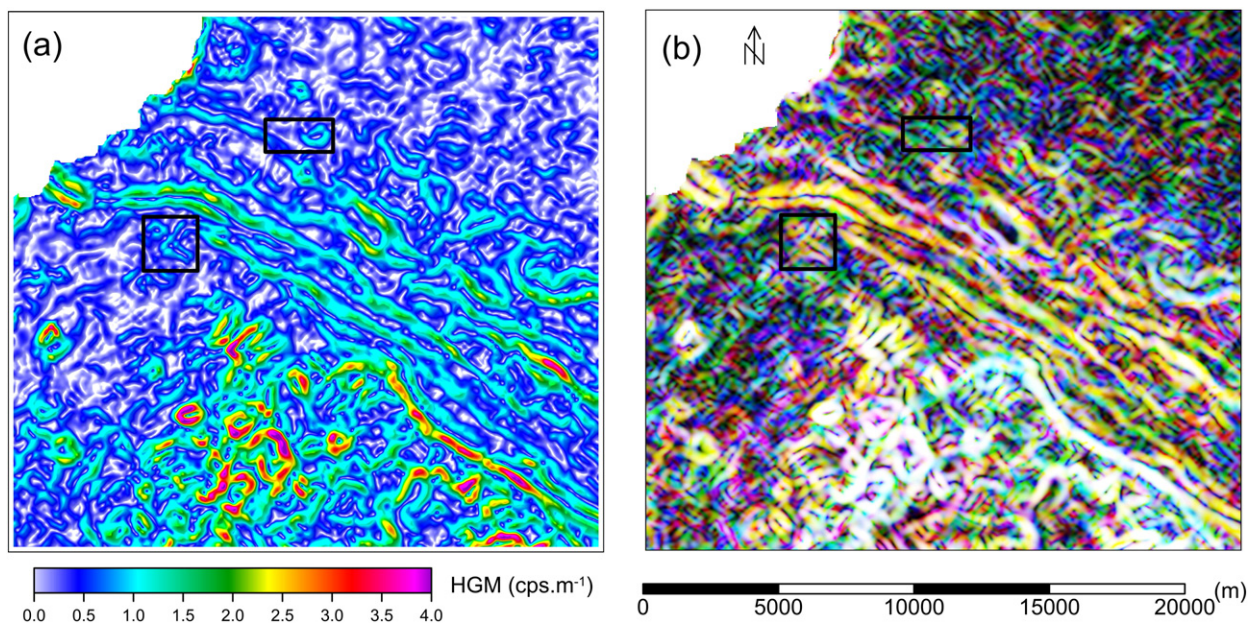


Fig. 12. The 22×20 km main study area. The 2 rectangles are referred to in the text. (a) Continuous colour image, with shade, of the horizontal gradient magnitude (HGM) obtained from the TC data. (b) Ternary image of the HGM of potassium (red), HGM of thorium (green) and HGM of uranium (blue).

with the northern and eastern granite edge. The spectral behaviour assists with the identification of potential continuity of edge effects.

The TC-HGM response of Fig. 12a contains a noise level that can be associated with the lowest amplitudes. This information is not immediately apparent in the ternary-HGM of Fig. 12b and so it may be prudent to assess their joint behaviour. In order to introduce a noise assessment into the images of Fig. 12 it is possible to blank regions (grid cells) falling below a selected amplitude threshold. In the case of the Fig. 12a this would be based on the TC-HGM amplitude. In the case of Fig. 12b, the same procedure can be transferred to the ternary image or a different threshold can be developed using the amplitudes, or amplitude combinations, of the 3 radioelement HGM amplitudes. Much of the detailed behaviour in Fig. 12 does not have a random (noise) appearance. The character of the edges detected will be governed by the limits to spatial resolution of finite areas that were discussed, both theoretically and empirically, previously. Many of the localised responses are likely to be soil related. Two rectangles, displaying such effects, allow the slightly different character of the two responses to be compared. Much soil mapping is based on texture whereas the flux changes assessed here largely relate to changes in soil properties (in the absence of bedrock effects). According to Beamish (2015), the main soil properties involved are density and wetness.

6. Conclusions

The theoretical results of the study indicate that 90% of the total flux is obtained across ground scale lengths of 250 m (60 m elevation), 360 m (120 m elevation) and 440 m (180 m elevation). The airborne measurements therefore constitute a moving-average spatial measurement thus limiting precise resolution of flux behaviour. A further study of anomalies of finite lateral extent indicated the decrease in flux count with survey elevation and a reduced response with decreasing source dimension. The detectability of small anomalous areas (<100 m, or half the flight line spacing) is likely to be low or non-existent. The results indicate that, for lateral dimensions greater than the flight line spacing, the lateral scale of the anomalous source response is governed by the scale length of the anomalous region. A study of the horizontal gradient magnitude (HGM) of the anomalous response indicated that the edges of the anomalous region could be identified as maxima in the HGM response. The technique therefore offers increased resolution of the lateral contributions to changes in flux behaviour.

A control study area containing isolated island responses of varying scale-lengths was used to further assess the HGM resolution characteristics using survey data. Small islands less than the flight-line spacing are not detected unless a survey line directly overflies the island. The intrinsic shape of larger features is only partially replicated and again demonstrates the limited detailed resolution characteristics of airborne survey data. Although the application of moving-window curvature analysis to the HGM response was demonstrated, a continuous image of the HGM response is potentially the most useful in providing the largest dynamic range of the behaviour generated by the lateral contrasts.

HGM analysis was applied to recent survey data to allow an assessment of geological, soil and environmental effects. The amplitudes of the data used must also be used to distinguish the form of the relative flux behaviour (i.e. an attenuation or enhancement). While at the large (survey-wide) scale, there is a clear association between major bedrock types and the radiometric spectral response, the high resolution HGM analysis reveals the extent of small scale contributions to the response. Such effects are pervasive and include contributions from bedrock lithologies, changes in soil properties, man-made soil removal (quarrying), water bodies and certain types of vegetation. These can be studied using the high signal total count data and/or the spectral response formed by the HGM response of individual radioelements.

Acknowledgements

My thanks go to Jim White for an internal review and to Joe Duval and the USGS for providing the software used in the theoretical study. Topographic map data used here are based upon Ordnance Survey data with the permission of the Controller of Her Majesty's Stationery Office, © Crown copyright. The Northern Island data used in the study come from the Tellus Project which was funded by DETI and by the Building Sustainable Prosperity scheme of the Rural Development Programme (Department of Agriculture and Rural Development of Northern Ireland). This paper is published with the permission of the Executive Director, British Geological Survey (NERC).

Appendix A. Supplementary data

Supplementary data associated with this article can be found in the online version, at doi:<http://dx.doi.org/10.1016/j.jappgeo.2016.07.006>. These data include Google maps of the most important areas described in this article.

References

- Beamish, D., 2012. The application of spatial derivatives to non-potential field data. *Geophys. Prospect.* 60, 337–360.
- Beamish, D., 2013. Gamma ray attenuation in the soils of Northern Ireland, with special reference to peat. *J. Environ. Radioact.* 115, 13–27.
- Beamish, D., 2014. Peat mapping associations of airborne radiometric survey data. *Remote Sens.* 6, 521–539.
- Beamish, D., 2015. Relationships between gamma-ray attenuation and soils in SW England. *Geoderma* 259–260, 174–186.
- Beamish, D., White, J.C., 2011. A radiometric airborne geophysical survey of the Isle of Wight. *Proc. Geol. Assoc.* 122, 787–799.
- Beamish, D., White, J., 2014. TellusSW: airborne geophysical data and processing report. *British Geological Survey Open Report, OR/14/014*.
- Beamish, D., Young, M., 2009. Geophysics of Northern Ireland: the Tellus effect. *First Break* 27, 43–49.
- Blakely, R.J., 1995. *Potential Theory in Gravity and Magnetic Applications*. Cambridge University Press, Cambridge, U.K.
- Blakely, R.J., Simpson, R.W., 1986. Approximating edges of source bodies from magnetic or gravity anomalies. *Geophysics* 51, 1494–1498.
- Dickson, B.L., Scott, K.M., 1997. Interpretation of aerial gamma-ray surveys – adding the geochemical factors. *AGSO J. Aust. Geol. Geophys.* 17, 187–200.
- Duval, J.S., 1997. Gamma-ray modelling programs. *U.S. Geol. Surv. Open File Rep.* 97–96.
- Duval, J.S., Cook, B., Adams, J.A.S., 1971. Circle of investigation of air-borne gamma-ray spectrometer. *J. Geophys. Res.* 76, 8466–8470.
- Edmonds, E.A., McKeown, M.C., Williams, M., 1975. *British Regional Geology: South-West England*. fourth ed. HMSO, London.
- Grasty, R.L., Minty, B.R.S., 1995. A guide to the technical specifications for airborne gamma-ray surveys. *AGSO Australian Geological Survey Organisation, Record 1996/60*.
- Grauch, V.J.S., Hudson, M.R., Minor, S.A., 2001. Aeromagnetic expression of faults that offset basin fill, Albuquerque basin, New Mexico. *Geophysics* 66, 707–720.
- IAEA, 1991. *Airborne Gamma Ray Spectrometer Surveying*. Technical Report Series/International Atomic Energy Agency, Vienna (No. 323).
- IAEA, 2003. *Guidelines for Radioelement Mapping Using Gamma Ray Spectrometry*. Technical Report Series/International Atomic Energy Agency, Vienna (No. 136).
- IAEA, 2010. *Radioelement Mapping*. Nuclear Energy Series/International Atomic Energy Agency, Vienna (No. NF-T-1.3).
- Kimbell, S.F., Cooper, D.C., Scrivener, R.C., 2003. The digitisation and geological interpretation of data from the 1957–9 airborne radiometric survey of south-west England. *Geoscience in South-West England*. 10, pp. 410–416.
- Leveridge, B.E., Hartley, A.J., 2006. The Variscan orogeny: the development and deformation of Devonian/Carboniferous basins in SW England and South Wales. In: Brenchley, P.J., Rawson, P.F. (Eds.), *The Geology of England and Wales*, second ed. Geological Society, London, pp. 225–255.
- Minty, B.R.S., 1967. Fundamentals of airborne gamma-ray spectrometry. *AGSO J. Aust. Geol. Geophys.* 17, 39–50.
- Nabighian, M.N., Grauch, V.J.S., Hansen, R.O., LaFehr, T.R., Li, Y., Peirce, J.W., Phillips, J.D., Ruder, M.E., 2005. The historical development of the magnetic method in exploration. *Geophysics* 70, 33–61.
- Peart, R.J., Cuss, R.J., Beamish, D., Jones, D.G., 2003. The High Resolution Airborne Resource and Environmental Survey-Phase 1 (HiRES-1): Background, Data Processing and Dissemination and Future Prospects. *British Geological Survey Internal Report IR/03/112*.
- Phillips, J.D., Hansen, R.O., Blakely, R.J., 2007. The use of curvature in potential-field interpretation. *Explor. Geophys.* 38, 111–119.
- Pitkin, J.A., Duval, J.S., 1980. Design parameters for aerial gamma ray surveys. *Geophysics* 45, 1427–1439.
- Wilford, J.R., Bierworth, P.N., Craig, M.A., 1997. Application of airborne gamma-ray spectrometry in soil/regolith mapping and applied geomorphology. *AGSO J. Aust. Geol. Geophys.* 17, 201–216.